

# Anomalous collective diffusion of interacting self-propelled particles

Tanmoy Chakraborty and Punyabrata Pradhan

*Department of Physics of Complex Systems, S. N. Bose National Centre for Basic Sciences,  
Block-JD, Sector-III, Salt Lake, Kolkata 700106, India*

We characterize collective motion of strongly persistent interacting self-propelled particles (SPPs) and offer a generic mechanism by using the characteristics of nonlinear diffusion, that accounts for the early-time anomalous relaxations observed in such systems. For small tumbling rate  $\gamma \ll 1$ , a suitably scaled bulk-diffusion coefficient  $\mathcal{D}(\rho, \gamma)$ , as a function of density  $\rho$ , is found to vary as a power law in a broad range of density:  $\mathcal{D} \propto \rho^{-\alpha}$ , with exponent  $\alpha$  slowly crossing over from  $\alpha = 2$  at large densities to  $\alpha = 0$  at small densities. As a result, the density relaxation is governed by a nonlinear diffusion equation, exhibiting anomalous spatio-temporal scaling, which, in certain regimes, is ballistic. We rationalize these findings through a scaling theory and substantiate our claims by directly calculating the bulk-diffusion coefficient in two minimal models of SPPs, for arbitrary density  $0 < \rho < 1$  and tumbling rate  $\gamma > 0$ . We show that, for  $\gamma \ll 1$ , the bulk-diffusion coefficient has a scaling form  $\mathcal{D}(\rho, \gamma) = \gamma^{-2} \mathcal{F}(\rho/\gamma)$ , where the scaling function  $\mathcal{F}(\psi)$  is analytically calculated for one model and numerically for the other. Our arguments are rather generic, being independent of dimensions and microscopic details.

*Introduction.*— Transport characteristics of self-propelled particles (SPPs) never cease to surprise [1]; indeed, they are quite often anomalous, indicating the presence of nontrivial correlations and serving as the rule rather than the exception. Anomalous transport in such systems, which range from living to non-living matter (e.g., bacterial colonies and active janus particles, respectively), has generated a lot of interest and has been investigated in a variety of experiments [2–9], simulations [10, 11], and theory [12–15]. For instance, a recent experiment on the expansion of localized janus swimmers on a two-dimensional substrate was found to exhibit an early-time ballistic growth [16], characterized by the dynamic exponent  $z = 1$  (ultimately crossing over to normal diffusion with  $z = 2$ ). In a related simulation study of single-file transport of interacting SPPs, the space-time scaling of the two-point density correlations in the early-time regimes was shown to display superdiffusion with  $z \approx 1.67$  [17]. At this time, it is unclear precisely what causes the anomalous growth, the resultant exponent, and whether or not one should expect a universal behavior. A good theoretical understanding of the time-dependent properties of interacting SPPs, taking into consideration the *many-body correlations*, is, in fact, still missing, despite significant advances achieved recently [18–21]. In this letter, starting with a many-particle description, we present a hitherto unexplored hydrodynamic theory that describes the remarkable collective relaxations seen in SPPs.

The efforts in understanding the time-dependent properties in such systems have generally been streamlined into addressing a particular aspect of the problem, i.e., characterizing the self-diffusion coefficient of tracer particles and related quantities, such as the intermediate scattering function [14, 22–29]. However, for standard models of SPPs [23, 30–34], a rigorous microscopic dynamical theory of collective diffusion and large-scale relaxations, characterized by another transport coefficient called the *bulk-diffusion coefficient*, remains largely un-

explored [35]. In this scenario, a theoretical investigation of the relaxation processes in interacting SPPs is perhaps long overdue. Notably, the self-diffusion coefficient and the bulk-diffusion coefficient are in principle different; in fact, they can have quite contrasting behaviors, e.g., while the former is expected to vanish upon approaching the maximum permissible density, the latter could still remain nonzero [36].

In this Letter, we theoretically investigate bulk-diffusion in *strongly persistent* interacting SPPs. Our theory is simply understood through a generic scaling argument, that is independent of dimensions and microscopic details, and it unveils a unique mechanism of particle transport in these systems. Our central idea is that the transport in the limit of strong persistence is actually governed by two microscopic length scales, the “mean free path” and the persistence length; as a result, the bulk-diffusion coefficient has a highly nonlinear (power-law) density dependence, accounting for the previously observed early-time anomalous growth. We show that the density profiles at early times are *non-Gaussian*, where their spatio-temporal scaling form can be determined within the theory. Furthermore, our findings suggest that the related growth exponent is *not* universal and is dependent on specific parameter regimes.

The SPPs move ballistically with a characteristic speed  $v$  (called “run”) and randomly change direction (called “tumble”) with a certain rate  $\gamma = 1/\tau_p$ , where  $\tau_p$  is a typical persistence time (equivalent to a persistence length  $l_p = v\tau_p$ ). Particles also interact with their neighbors, for example, through excluded-volume, or hardcore, interactions, as discussed here. We do not, however, consider thermal diffusion, which is irrelevant in the strong-persistence regime. Furthermore, in the hydrodynamic theory developed here, the large system-size limit is taken first, followed by the large persistence-time limit; limits should be taken in this order only, as doing the opposite leads to jammed configurations.

Let us begin by discussing the scaling argument and

the nonlinear diffusion mechanism. For simplicity, consider  $N$  hardcore particles on  $d$ -dimensional periodic square lattice of size  $L$  and volume  $V = L^d$  where fraction of occupied sites (“volume fraction”), or the number density,  $\rho = N/V$ . The propulsion directions of particles randomly orient towards any of the  $2d$  possible directions. Particles collide and become locked (jammed) due to hardcore interactions and opposite propulsion directions; eventually, unlocking events occur, allowing the particles to travel ballistically again, and so on. We note that there are only two relevant length scales in the problem: The *persistence length*  $l_p = v/\gamma$  and the *mean free path*. In fact, in the *strong-persistence* limit, the mean free path traversed by a particle before colliding with the next particle is the mean gap  $\langle g \rangle$  between particles (inter-particle spacing). As a result, any quantities must be constructed from simple dimensional ground by combining the three microscopic parameters:  $l_p$ ,  $\langle g \rangle$  and  $v$ . This implies that the bulk-diffusion coefficient can be cast in a form  $D = (v^2/\gamma)\mathcal{F}(v/\langle g \rangle\gamma)$ , where scaling function  $\mathcal{F}(\psi)$  depends on a *single* dimensionless scaling variable  $\psi = v/\langle g \rangle\gamma = l_p/\langle g \rangle$ ; evidently, the prefactor  $v^2/\gamma$  gives right dimension of  $D$ . Furthermore, as the average number of particles in any row (consisting of  $L$  sites) is equal to  $L/\langle g \rangle$  and therefore  $(L/\langle g \rangle) \times L^{d-1} = N$ , we obtain, in the limit of low density, an exact relation,

$$\langle g \rangle = \frac{1}{\rho}, \quad (1)$$

which, remarkably, depends *only* on density, *not* on tumbling rate and dimensions. We then write the bulk-diffusion coefficient in a slightly different form,

$$D(\rho, \gamma) = \frac{1}{\gamma}\mathcal{F}\left(\frac{\rho}{\gamma}\right) \equiv l_p\mathcal{F}(l_p\rho), \quad (2)$$

with  $\psi = \rho/\gamma = l_p\rho$ ; without loss of generality, we put  $v = 1$  throughout. The asymptotic form of  $\mathcal{F}(\psi)$  is determined as follows. In the *noninteracting* limit  $\rho \rightarrow 0$  and  $l_p/\langle g \rangle \rightarrow 0$ , we have  $D \sim 1/\gamma$ , implying  $\mathcal{F}(\psi) = \text{const.}$  as  $\psi \rightarrow 0$ . However, in the *interacting* limit  $l_p/\langle g \rangle \rightarrow \infty$ ,  $D$  is proportional to  $\gamma$  as microscopic events occur on a time scale  $\tau_p = \gamma^{-1}$ , implying  $\mathcal{F}(\psi) \sim 1/\psi^2$  as  $\psi \rightarrow \infty$ . This explains the power-law dependence of  $D$  on  $\rho$  and, as we show later, the anomalous early-time relaxations.

The above argument, although plausible, must be validated in specific models, which we accomplish next in the context of two minimal models by obtaining their hydrodynamics.

*Hydrodynamics.*— Hydrodynamics deals with large-scale spatio-temporal properties of slow variable(s). As particle-number is conserved, on a time scale much larger than the persistence time  $\tau_p = \gamma^{-1}$ , number density  $n(X, t)$ , at position  $X$  at time  $t$ , is the only slow variable in the system. In that case, effective density relaxation is governed by diffusion processes and one can then define a density-dependent bulk-diffusion coefficient  $D(n, \gamma)$ , through a constitutive relation between the local

diffusive current  $J$  and density  $n$ ,

$$J(X, t) = -D(n, \gamma)\frac{\partial n}{\partial X}. \quad (3)$$

From continuity equation  $\partial\rho/\partial t + \partial J/\partial X = 0$ , we immediately obtain the time-evolution of local density,

$$\frac{\partial n(X, t)}{\partial t} = \frac{\partial}{\partial X} \left[ D(n, \gamma)\frac{\partial n}{\partial X} \right], \quad (4)$$

which, due to an explicit density dependence of the bulk-diffusion coefficient, is governed by a nonlinear diffusion equation and, as we discuss later, has interesting consequences. Now, by using the hydrodynamic (diffusive) scaling  $x = X/L$  and  $\tau = \gamma t/L^2$  and rescaling density, current and diffusion coefficient as  $n(X, t) = \rho(X/L, \gamma t/L^2)$ ,  $J(X, t) = L^{-1}j(X/L, \gamma t/L^2)$ , and  $D(n, \gamma) = \gamma\mathcal{D}(\rho, \gamma)$ , respectively, we obtain hydrodynamic evolution of the density field,

$$\frac{\partial\rho(x, \tau)}{\partial\tau} = \frac{\partial}{\partial x} \left[ \mathcal{D}(\rho, \gamma)\frac{\partial\rho(x, \tau)}{\partial x} \right]. \quad (5)$$

We verify the hydrodynamic description for two minimal models of interacting SPPs, having the following *necessary ingredients* - (i) a typical persistence length  $l_p = \gamma^{-1}$  and (ii) excluded-volume interaction.

*Lattice gas with long-ranged hopping.*— Let us first consider a lattice gas model of  $N$  hardcore particles on a ring of  $L$  sites. With unit rate, a particle attempts to hop, symmetrically in either direction, by hop-length  $l$  drawn from an exponential distribution  $\phi(l) \propto \exp(-l/l_p)$ . Provided that the stretch of consecutive vacancies, called the *gap*, in front of the particle is at least of length  $l$  (i.e., if gap size  $g \geq l$ ), the attempted hop is successful; otherwise, due to the hard-core constraints, the particle traverses the entire stretch and sits adjacent to its nearest occupied site. Clearly, the long-ranged hopping mimics ballistic “run” of micro-swimmers, having random (exponentially distributed) “run”-lengths, with a typical persistence length  $l_p$  and is expected to capture collective behavior of RTPs on the persistence time-scale  $\tau_p$ . The model is clearly an idealized representation of more realistic systems of interacting SPPs. Despite the simplicity, its steady-state measure is not a product one and generates nontrivial spatial correlations that are long-ranged for large persistence lengths, resulting in clustering, huge density fluctuations, and dynamical heterogeneity.

*Bulk-diffusion coefficient.*— A great advantage in dealing with such lattice gases is that the system possesses a generalized *gradient property* [36], which allows for local instantaneous current to be expressed as the gradient of a local observable and for the bulk-diffusion coefficient to be exactly determined in terms of the steady-state gap distribution  $P(g)$ . We provide below a sketch of our calculation method and the main results; see Appendix A for details. The main quantity of interest here is the average time-integrated current  $\langle Q_X(t) \rangle$ , where  $Q_X(t)$  is the cumulative current across a bond  $(X, X + 1)$  up to

time  $t$ . Then the time derivative  $d\langle Q_X(t) \rangle / dt$  gives the instantaneous coarse-grained current, which is shown to be diffusive in nature and, by using Eq. (3), we can immediately express the bulk-diffusion coefficient as

$$\mathcal{D}_{LH}(\rho, \gamma) = -\frac{1}{2} \frac{\partial(\rho u)}{\partial \rho}, \quad (6)$$

where the function

$$u(\rho, \gamma) = \sum_{l=1}^{\infty} \phi(l) \left( \sum_{g=1}^{l-1} gP(g) + l \sum_{g=l-1}^{\infty} (g-l+1)P(g) \right) \quad (7)$$

depends on both density and persistence length  $l_p = \gamma^{-1}$ . Of course, exact calculation of gap distribution  $P(g)$  is difficult in general. However, under a quite general condition,  $P(g)$  for large  $g$  can be well approximated by an exponential function,

$$P(g) \simeq N_* e^{-g/g_*}, \quad (8)$$

where  $N_*$  and  $g_*$  are the proportionality constant and the typical gap size, respectively, and both depend on  $\rho$  and  $\gamma$ ;  $N_*$  can be determined from the normalization condition  $\sum_g P(g) = 1$  and  $\langle g \rangle \simeq 1/\rho$ . Now following the previously mentioned scaling argument, the typical gap size is expected to have a scaling form,

$$g_* \simeq \frac{1}{\rho} \mathcal{G}(\psi), \quad (9)$$

with  $\psi = \rho/\gamma = l_p \rho$ ; this assertion has been explicitly checked in simulations (see Appendix B). The prefactor in the rhs of eq.(29) is fixed from the fact that, in the limit  $\psi \rightarrow 0$ , the system reduces a noninteracting one and therefore  $\mathcal{G}(0) = 1$  [37].

Also, in this limit, it can be checked that  $u = (1/\rho - 1)$  and, from eq.(6)  $D = \text{const.}$  - the standard result for symmetric simple exclusion process. In the opposite limit of  $\psi$  large, as shown in [38], the gap size is given by  $g_* = \sqrt{\psi}/\rho$ . Combining the two limiting behaviors provides, we have  $\mathcal{G}(\psi) \simeq (1 + \psi)^{1/2}$ . Most interestingly, we show that there exists a scaling limit of  $\gamma \rightarrow 0$  and  $\rho \rightarrow 0$  with  $\psi = \rho/\gamma$  fixed, for which the scaled bulk-diffusion coefficient  $\gamma^2 \mathcal{D}_{LH}(\rho, \gamma)$  from eqs.(6) and (7) is a function of a single scaling variable  $\psi$ ,

$$\mathcal{D}_{LH}(\rho, \gamma) = \frac{1}{\gamma^2} \mathcal{F}_{LH}(\psi), \quad (10)$$

where

$$\mathcal{F}_{LH}(\psi) = \frac{\mathcal{G}^2(\psi)}{(\mathcal{G}(\psi) + \psi)^3} \left( 1 - \psi \frac{\mathcal{G}'(\psi)}{\mathcal{G}(\psi)} \right); \quad (11)$$

see Appendix C for details. For the lattice gas studied here, we use the above mentioned form of  $\mathcal{G}(\psi) \simeq (1 + \psi)^{1/2}$  in eq.(11), to explicitly obtain

$$\mathcal{F}_{LH}(\psi) = \frac{(2 + \psi)}{2(\psi + \sqrt{1 + \psi})^3}, \quad (12)$$

which is the first main result of the Letter. Note that, for  $\psi \ll 1$ ,  $\mathcal{F}(\psi) = 1$  and consequently  $\mathcal{D}_{LH} \simeq 1/\gamma^2$ , which however diverges when the persistence length diverges; for  $\psi \gg 1$ ,  $\mathcal{F}(\psi) \simeq 1/2\psi^2$  and  $\mathcal{D}_{LH} \simeq 1/2\rho^2$ . In Fig. 1, we plot  $\gamma^2 \mathcal{D}_{LH}$  as a function of  $\rho/\gamma$ , by numerically calculating  $\mathcal{D}_{LH}$  from eqs.(6) and (7) through  $P(g)$  obtained from simulations (points), see Appendix A. We observe a nice scaling collapse, having an excellent agreement with theory eq.(12) (black line). Also, through numerical integration of eq.(5), we independently check eq.(6) by time-evolving various initial density profiles, thus confirming the validity of diffusive scaling used to obtain eq.(5) (see Appendix F for details).

*Model of RTPs.* - Next we study the paradigmatic model of hardcore run-and-tumble particles (RTPs), each of which is associated with a spin variable, on a one dimensional periodic lattice of  $L$  sites [30]. A particle hops to its nearest-neighbor with unit rate along its spin direction (run), provided the destination site is vacant, and, with rate  $\gamma$ , its spin flips (tumble). Between two successive spin-flips occurring on a scale of persistence time  $\tau_p = 1/\gamma$ , a particle would perform a run of length  $l$  (provided an empty stretch available), typically having an exponentially distribution (as considered in the lattice gas discussed above). Indeed, the lattice-gas and RTP models have remarkably similar features, which is evident upon a suitable rescaling in the RTPs:  $\gamma t \rightarrow t$  and consequently  $D_{RTP} \rightarrow \gamma \mathcal{D}_{RTP}$ , i.e., by measuring time in the unit of persistence time  $\tau_p = \gamma^{-1}$  (see Figs. 1 and 2); here  $\mathcal{D}_{RTP}$  is the bulk-diffusion coefficient for the RTPs. Now, according to our scaling argument, in this case too, the scaled bulk-diffusivity  $\gamma^2 \mathcal{D}_{RTP} = \mathcal{F}_{RTP}(\rho/\gamma)$  should be expressed in terms of a scaling function, as in eq.(10), which we check next. As an analytic calculation of  $\mathcal{D}_{RTP}$  for arbitrary densities and tumbling rates is challenging [39], here we resort to a computationally efficient simulation technique described below [40].

*Bulk-diffusion coefficient of RTPs.* - To this end, we study the relaxation dynamics of a long wave-length (sinusoidal) initial density perturbation  $\delta\rho(x, 0) = \rho(x, 0) - \rho_0 \equiv A(0) \sin(2\pi x)$ , with wave number  $2\pi/L$ , lattice position  $X = xL$  and  $\rho_0$  a uniform background density, around which the perturbation is applied. In the limit of weak perturbation  $A(0) \ll \rho_0$ , the density profile at sufficiently large time  $t = \tau L^2$  can be written as  $\delta\rho(x, \tau) = A(\tau) \sin(2\pi x)$ , with  $A(\tau) = A(0)e^{-\Gamma\tau}$  and the relaxation rate  $\Gamma(\rho_0, \gamma) = 4\pi^2 \mathcal{D}_{RTP}(\rho_0, \gamma)$ . In simulations, we measure the relaxation rate and obtain the bulk-diffusion coefficient from the relation  $\mathcal{D}_{RTP} = \Gamma/4\pi^2$  (see Appendix D, E for details). To ensure diffusive relaxation, one should first take the thermodynamic limit ( $L, N \rightarrow \infty$  with  $\rho = N/L$  fixed) and then vary the tumbling rate  $\gamma$  and analyze the case of  $\gamma \ll 1$  (in the opposite order of limit, where  $\gamma \rightarrow 0$  first and then  $L \rightarrow \infty$ , the system goes into a ‘‘jammed’’ or an ‘‘absorbing’’ state).

We observe that persistence and hard-core interaction compete with each other: While the former enhances diffusion, the latter diminishes it, resulting in nonmono-

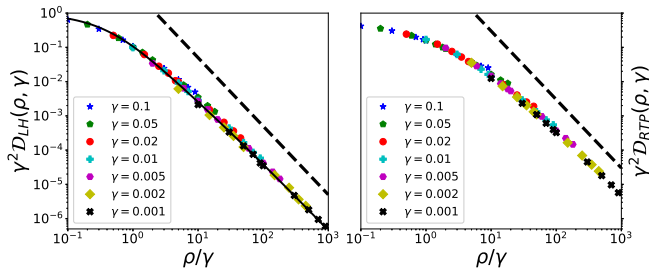


FIG. 1. *Scaling collapse of bulk-diffusion coefficient.* Scaled bulk-diffusion coefficients  $\gamma^2 \mathcal{D}(\rho, \gamma)$  are plotted as a function of the scaled variable  $\psi = l_p \rho = \rho/\gamma$  for the lattice gas (left panel) and RTPs (right panel). The overlapping solid line at the left panel represents the theoretically obtained scaling function  $\mathcal{F}_{LH}(\psi)$  shown in eq. (12)), while the black dotted guiding line in both these panels are showing the universal  $1/\psi^2$  behaviour of  $\mathcal{F}(\psi)$  at large  $\psi$ .

tonic variation of the *unscaled* diffusivity,  $D_{RTP}(\rho, \gamma) = \gamma \mathcal{D}_{RTP}(\rho, \gamma)$ , as a function of tumbling rate  $\gamma$  (see Appendix E for details). Notably, a similar feature is observed in the lattice gas model upon tuning persistence length  $l_p = \gamma^{-1}$ . However, as argued before and demonstrated for the lattice gas, one can in fact quantify this fascinating interplay between persistence and interaction through the scaling variable  $\psi = \rho/\gamma$  for the RTPs too. In Fig. 1, we plot  $\gamma^2 \mathcal{D}_{RTP}(\rho, \gamma) \equiv \mathcal{F}_{RTP}(\psi)$  as a function of  $\psi = \rho/\gamma$  and observe an excellent scaling collapse, even in the relatively large-density regime. Moreover, as in the lattice gas model, we find that  $\mathcal{F}_{RTP}(0) = \text{const.}$  and  $\mathcal{F}_{RTP}(\psi) \simeq 1/\psi^2$  for  $\psi \gg 1$ .

Note that, strictly in the limit  $\gamma \rightarrow 0$ , the hydrodynamics for RTPs are not well defined unless time and density are appropriately scaled; this is because the (unscaled) bulk-diffusion coefficient  $D(\rho, \gamma) \sim 1/\gamma$  diverges as  $\rho \rightarrow 0$  and  $D(\rho, \gamma) \rightarrow 0$  for any finite  $\rho$ . We therefore scale density and time,  $\psi(x, \tilde{\tau}) = \rho(x, \tau)/\gamma$  and  $\tilde{\tau} = \tau/\gamma^2$ , respectively, in order to have a well-defined hydrodynamic equation,

$$\frac{\partial \psi(x, \tilde{\tau})}{\partial \tilde{\tau}} = \frac{\partial}{\partial x} \left[ \mathcal{F}_{RTP}(\psi) \frac{\partial \psi(x, \tilde{\tau})}{\partial x} \right], \quad (13)$$

our second main result. The lattice gas model has a similar hydrodynamic equation, in the limit  $l_p \rightarrow \infty$ , obtained by replacing  $\mathcal{F}_{RTP}(\psi) \rightarrow \mathcal{F}_{LH}(\psi)$ ; see Appendix G for details.

*Anomalous (superdiffusive) transport.*— Finally we analyze the issue of anomalous time-evolution of initially localized density profiles in these two models. We first note that, depending on the density and tumbling rate (typically small), the bulk-diffusion coefficient can have a power-law dependence on density, i.e.,  $\mathcal{D}(n) \simeq C/n^\alpha$ , where the constant  $C$  and  $\alpha$  ( $0 \leq \alpha < 2$ ) depends on the parameter regime under consideration. Then the time-evolution equation (4), for the initial condition  $n(X, 0) = n_1 \delta(X)$ , can be exactly solved through a scaling ansatz  $n(X, t) = (Ct)^{-\omega} \mathcal{R}(\xi)$ . Upon substituting the ansatz

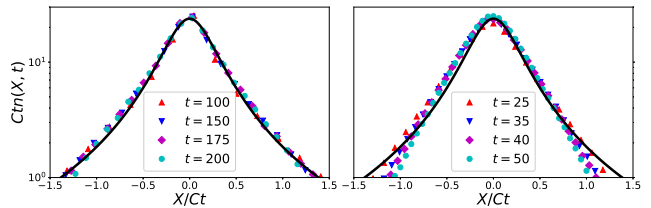


FIG. 2. *Verification of the scaling solution in Eq. (14).* We plot the scaled density profile  $Ctn(X, t)$  against the scaled variable  $\xi = X/Ct$  for the lattice gas (left-panel) and RTPs (right-panel) at various microscopic times  $t$ . We fix the spin-flipping rate at  $\gamma = 0.05$  i.e.  $l_p = 20$  with the corresponding  $C = 2.2$  (for lattice gas) and 3.2 (for RTPs). The black solid-line is the scaling solution  $\mathcal{R}(\xi)$  defined in Eq. (14). We find a good agreement between simulation data points and the scaling solution  $\mathcal{R}(\xi)$ .

in eq.(4), we get an equation  $\omega [\xi \mathcal{R}(\xi)]' = -[\mathcal{R}^{-\alpha} \mathcal{R}'(\xi)]'$  for  $R(\xi)$  (“prime” denotes derivative wrt  $\xi$ ) in terms of a *single* variable  $\xi = X/(Ct)^\omega$ , implying the growth exponent  $\omega = 1/(2 - \alpha)$  (see Appendix I). For the purpose of demonstration, we choose a regime where  $\alpha = 1$  and consequently  $\omega = 1$  (thus the dynamic exponent  $z = 1/\omega = 1$ ), implying a ballistic transport, quite strikingly within a framework of a diffusion equation (4), albeit a nonlinear one. Now, by using conditions  $\mathcal{R}(0) = 2/\xi_0^2$  and  $\mathcal{R}'(0) = 0$ , we exactly solve for

$$\mathcal{R}(\xi) = \frac{2}{(\xi_0^2 + \xi^2)}, \quad (14)$$

with constant  $\xi_0$  fixed through conservation condition  $\int_{-\infty}^{\infty} \mathcal{R}(\xi) d\xi = \text{const.}$ ; particularly, for  $\xi \gg 1$ ,  $R(\xi) \sim 1/\xi^2$  - a power law. Thus the density relaxation has anomalous spatio-temporal scaling with a non-Gaussian spread, which however eventually becomes Gaussian (thus normal diffusion with  $z = 2$ ). In Fig. 2, we plot the scaled density profile  $Ctn(X, t)$ , obtained from simulation, as a function of  $X/Ct$  in the early-time (still relatively large) regime; we have a nice scaling collapse and a reasonable agreement with theory eq. (14), our third main result.

*Summary.*— In conclusion, we provide a hydrodynamic theory, that accounts for anomalous transport observed in *strongly persistent* interacting SPPs. Indeed, the collective transport is caused by subtle many-body effects, that arise from an intriguing interplay between interaction and persistence and manifest themselves through competition between the two length scales - the mean gap (equivalently, mean free path) and the persistence length. We demonstrate this in two idealized models of SPPs by directly calculating the bulk-diffusion coefficients. Physically, local structural relaxations are sensitive to local densities and produce a wide range of time scales (power-law distributed), resulting in dynamical heterogeneity and nontrivial spatio-temporal correlations. Two remarks are in order. First and foremost, the hydrodynamic limit for small tumbling rate, which,



crucially, is independent of system size, differs from that investigated in Refs. [19, 21]. In fact, attempts to develop a rigorous hydrodynamic description of the standard versions of SPPs [23, 30–34], that correspond to this specific order of limit, has not been successful so far. Second, the bulk-diffusion coefficient investigated in this study remains interestingly nonzero throughout, in contrast to the self-diffusion coefficient, which vanishes as density  $\rho \rightarrow 1$  in hard-core lattice gases [24, 27], examined in a relatively similar context as addressed here. In light of the above, we believe our proposed mechanism of density relaxations in SPPs, which is quite broad and applicable to similar systems in general, could be useful.

*Acknowledgement.*—We thank Subhadip Chakraborti, Arghya Das, Rahul Dandekar and R. Rajesh for discussions. P.P. gratefully acknowledges the Science and Engineering Research Board (SERB), India, under Grant No. MTR/2019/000386, for financial support. T.C. acknowledges a research fellowship [Grant No. 09/575 (0124)/2019-EMRI] from the Council of Scientific and Industrial Research (CSIR), India.

## APPENDIX

### A. Derivation of the bulk-diffusion coefficient for lattice gas for arbitrary density and persistence length

Here we are going to calculate the time rate of change of the instantaneous bond current and use Eq. (3) in the main text to identify the bulk-diffusion coefficient  $\mathcal{D}_{LH}(\rho, \gamma)$  for the lattice gas model. Note that, whenever a particle performs long-range hop to reach the destination site, it overtakes all the vacant sites in the midway of its journey and for a rightward (leftward) hop, current across all such bonds increases (decreases) by unity. To this end, we introduce the operators,

$$\hat{\mathcal{U}}_{X+l}^{(l)} = \bar{\eta}_{X+1} \bar{\eta}_{X+2} \cdots \bar{\eta}_{X+l}, \quad (15)$$

$$\hat{\mathcal{V}}_{X+l+1}^{(l+2)} = \eta_X \bar{\eta}_{X+1} \bar{\eta}_{X+2} \cdots \bar{\eta}_{X+l} \eta_{X+l+1}, \quad (16)$$

where  $\mathcal{U}^{(l)} = \langle \hat{\mathcal{U}}^{(l)} \rangle$  is the probability that consecutive  $l$  sites are vacant and  $\mathcal{V}^{(l+2)} = \langle \hat{\mathcal{V}}^{(l+2)} \rangle$  is the probability to observe a hole cluster of size  $l$ . If  $Q_l(X, t)$  is the time-integrated current across the bond  $(X, X+1)$  upto time  $t$  corresponding to the hop-length  $l$ , the total time-integrated current across the same bond, considering all possible hop-lengths, is defined as  $Q(X, t) = \sum_{l=1}^{\infty} Q_l(X, t) \phi(l)$ . It is to be noted that  $Q_X^{(l)}(t)$  increases due to rightward hopping events and for a fixed hop-length  $l$  and gap size  $g$ , we calculate the net probability of increment for the following two cases,

*Case I,  $l > g$ :* Here, in an infinitesimal time  $dt$ , particle crosses the entire cluster of holes of size  $g$  and consequently current across the  $g$  bonds inside the cluster are increased by unity. Therefore, for the increment of  $Q_X^{(l)}(t)$  due to the above move, the bond  $(X, X+1)$  must be within the hole cluster. However, we also realize that

a particular bond  $(X, X+1)$  can be retained inside a hole cluster of size  $g$  by translating the entire cluster in  $g$  possible ways and each of which corresponds to unit increment of  $Q_X^{(l)}(t)$ . The corresponding contribution to the probability is given by  $\mathcal{P}_{g,R}^> dt$  where,

$$\begin{aligned} \mathcal{P}_{g,R}^> &= \frac{1}{2} \sum_{k=1}^g \langle \eta_{X+k-g} \bar{\eta}_{X+k-g+1} \bar{\eta}_{X+k-g+2} \cdots \bar{\eta}_{X+k} \eta_{X+k+1} \rangle \\ &= \frac{1}{2} \sum_{k=1}^g \mathcal{V}_{X+k+1}^{(g+2)}. \end{aligned} \quad (17)$$

*Case II,  $l \leq g$  -* In this case, particle makes long hop along right by  $l$  distance in time  $dt$  and as a result, current across the  $l$  consecutive bonds along the hopping direction are increased by unity and  $Q_X^{(l)}(t)$  is increased by unity due to this move, if the bond  $(X, X+1)$  is a part of it. Alternatively, one may fix the bond  $(X, X+1)$  and translate the empty lane of size  $l$  with the hopping particle situated at the left most site in  $l$  possible ways and for each translation, current  $Q_X^{(l)}(t)$  increases by unit and the corresponding probability is  $\mathcal{P}_{g,R}^{\leq} dt$  and we calculate

$$\begin{aligned} \mathcal{P}_{g,R}^{\leq} &= \frac{1}{2} \sum_{k=1}^l \langle \eta_{X+k-l} \bar{\eta}_{X+k-l+1} \bar{\eta}_{X+k-l+2} \cdots \bar{\eta}_{X+k} \rangle \\ &= \frac{1}{2} \sum_{k=1}^l \left( \mathcal{U}_{X+k}^{(l)} - \mathcal{U}_{X+k}^{(l+1)} \right). \end{aligned} \quad (18)$$

Therefore, the total probability that corresponds to the increment of  $Q_X^{(l)}(t)$ , considering both the cases and all possible gap sizes, can be written as,

$$\begin{aligned} \mathcal{P}_R &= \sum_{g=1}^{\infty} \left[ \mathcal{P}_{g,R}^> \Theta(l-g) + \mathcal{P}_{g,R}^{\leq} (1 - \Theta(l-g)) \right] \\ &= \frac{1}{2} \left[ \sum_{g=1}^{l-1} \sum_{k=1}^g \mathcal{V}_{X+k+1}^{(g+2)} + \sum_{k=1}^l \left( \mathcal{U}_{X+k}^{(l)} - \mathcal{U}_{X+k}^{(l+1)} \right) \right]. \end{aligned} \quad (19)$$

Similarly, following the same method, the total probability corresponding to the unit decrement of  $Q_X^{(l)}(t)$ , in an infinitesimal time  $dt$ , due to leftward movement of the particle can be calculated to be,

$$\mathcal{P}_L = \frac{1}{2} \left[ \sum_{g=1}^{l-1} \sum_{k=1}^g \mathcal{V}_{X+k+1}^{(g+2)} + \sum_{k=1}^l \left( \mathcal{U}_{X+k}^{(l)} - \mathcal{U}_{X+k}^{(l+1)} \right) \right]. \quad (20)$$

Then the continuous-time evolution for the integrated current  $Q_X^{(l)}(t)$ , in an infinitesimal time interval  $dt$ , provided the hop-length is chosen to be  $l$ , can be written as follows:

$$\langle Q_X^{(l)}(t+dt) \rangle = \begin{cases} \langle Q_X^{(l)}(t) \rangle + 1, & \text{prob. } \mathcal{P}_R dt, \\ \langle Q_X^{(l)}(t) \rangle - 1, & \text{prob. } \mathcal{P}_L dt, \\ \langle Q_X^{(l)}(t) \rangle, & \text{prob. } 1 - \Sigma dt, \end{cases} \quad (21)$$

where the sum of probabilities for all possible ways the bond  $(X, X+1)$  changes current in the infinitesimal time interval  $dt$  is given by,

$$\Sigma = \frac{1}{2} \left[ \sum_{g=1}^{l-1} \sum_{k=1}^g \left( \mathcal{V}_{X+k+1}^{(g+2)} + \mathcal{V}_{X+k}^{(g+2)} \right) + \sum_{k=1}^l \left\{ \left( \mathcal{U}_{X+l-k}^{(l)} - \mathcal{U}_{X+l-k+1}^{(l+1)} \right) + \left( \mathcal{U}_{X+l-k}^{(l)} - \mathcal{U}_{X+l-k+1}^{(l+1)} \right) \right\} \right]. \quad (22)$$

Now, considering all possible hop-length  $l$  ranging from 1 to  $\infty$ , the time evolution of the average integrated current

$\langle Q_X(t) \rangle = \sum_{l=1}^{\infty} \phi(l) \langle Q_X^{(l)}(t) \rangle$  across  $(X, X+1)$  can be written as,

$$\frac{d\langle Q_X(t) \rangle}{dt} = \frac{1}{2} \sum_{l=1}^{\infty} \phi(l) \left[ \sum_{g=1}^{l-1} \left( \mathcal{V}_{X+g+1}^{(g+2)} - \mathcal{V}_{X+1}^{(g+2)} \right) + \left( \mathcal{U}_{X+l}^{(l)} - \mathcal{U}_X^{(l)} \right) \right]. \quad (23)$$

It is to be noted that the above equation is written in terms of the gradient of local observables. In the large time limit, we assume the observables to be slowly varying and the spatial variation of  $\mathcal{V}_X^{(g+2)}$  and  $\mathcal{U}_X^{(l)}$  is governed by the evolution of local density  $n(X, t) \equiv \rho$ . To this end, we can write  $\mathcal{V}_X^{(g+2)} \equiv \mathcal{V}^{(g+2)}(\rho)$  and  $\mathcal{U}_X^{(l)} \equiv \mathcal{U}^{(l)}(\rho)$  and consequently the gradient of local observables can be expressed as the gradient of local density  $\rho$ ,

$$\frac{d\langle Q_X(t) \rangle}{dt} = \frac{1}{2} \sum_{l=1}^{\infty} \phi(l) \left[ \sum_{g=1}^{l-1} g \frac{\partial \mathcal{V}^{(g+2)}(\rho)}{\partial \rho} + l \frac{\partial \mathcal{U}^{(l)}(\rho)}{\partial \rho} \right] \frac{\partial \rho}{\partial x}. \quad (24)$$

Comparing the above equation with Eq. (3) in the main text and identifying the correlators as a function of gap distribution function  $P(g|\rho)$  as,

$$\mathcal{V}^{(g+2)}(\rho) = \rho P(g|\rho), \quad (25)$$

$$\mathcal{U}^{(l)}(\rho) = \rho \sum_{g=l-1}^{\infty} (g-l+1) P(g|\rho), \quad (26)$$

the bulk-diffusion coefficient for the lattice gas model can be written as,

$$\mathcal{D}_{LH}(\rho, \gamma) = -\frac{1}{2} \frac{\partial}{\partial \rho} \left[ \rho \sum_{l=1}^{\infty} \phi(l) \left( \sum_{g=1}^{l-1} g P(g|\rho) + l \sum_{g=l-1}^{\infty} (g-l+1) P(g|\rho) \right) \right]. \quad (27)$$

This result is displayed in Eq. (6) and (7) in the main text. Along with the analytic calculation shown in the next section, here we opt for numerical simulation to calculate the bulk-diffusion coefficient  $\mathcal{D}_{LH}(\rho, \gamma)$ , which according to Eq. (27) essentially boils down in calculating the steady state gap size distribution  $P(g)$ . We numerically obtain  $P(g)$  and consequently  $\mathcal{D}_{LH}(\rho, \gamma)$  using Eq. (6) in the parameter range  $0.01 \leq \rho \leq 0.9$ ,  $0.001 \leq \gamma \leq 0.1$  for a fixed system size  $L = 3000$ . To compare with RTPs, in this section, we study the functional variation of the scaled bulk-diffusion coefficient  $\gamma \mathcal{D}_{LH}(\rho, \gamma)$ . At the left panel of Fig. 3 we plot

the  $\gamma \mathcal{D}_{LH}(\rho, \gamma)$ , as a function of the inverse persistence length  $l_p^{-1} = \gamma$  for various  $\rho = 0.01$  (blue square),  $0.05$  (red circle),  $0.1$  (black up-triangle) and  $0.5$  (magenta down-triangle). We observe the scaled bulk-diffusion coefficient  $\gamma \mathcal{D}_{LH}(\rho, \gamma)$  to be a non-monotonic function of the inverse persistence length  $\gamma$  and the nonmonotonicity effect is more pronounced at the lower density level. This nonmonotonicity is essentially due the intriguing interplay between persistence (induced by  $\gamma$ ) and the hard-core repulsive interaction (governed by  $\rho$ ). We will discuss this issue in detail in the next section. We also plot  $\gamma \mathcal{D}_{LH}(\rho, \gamma)$  against  $\rho$  at the right panel of Fig. 3

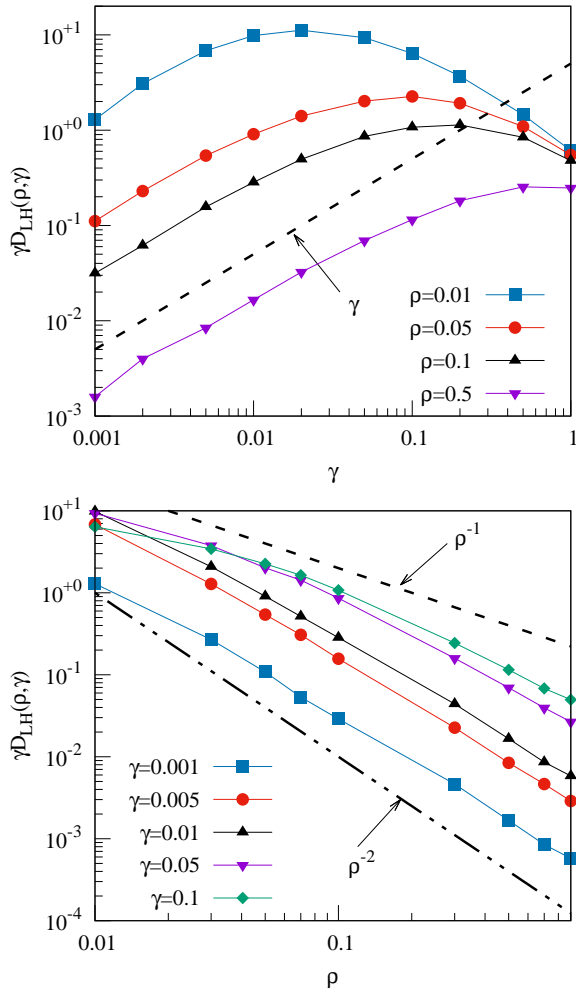


FIG. 3. *Bulk-diffusion coefficient for the lattice gas model.* We calculate the bulk-diffusion coefficient  $D(\rho, \gamma^{-1})$  for the lattice gas model using Eq. (6). In panel (a), we plot the scaled diffusion coefficient  $\gamma D(\rho, \gamma)$  as a function of the inverse typical hop-length  $\gamma$  for various density  $\rho = 0.01$  (blue square), 0.05 (red circle), 0.1 (black up-triangle), 0.5 (magenta down-triangle), while in panel (b),  $\gamma D(\rho, \gamma)$  is plotted against density  $\rho$  for different inverse typical hop-length  $\gamma = 0.001$  (blue square), 0.005 (red circle), 0.01 (black up-triangle), 0.05 (magenta down-triangle) and 0.1 (green tilted square).

for various  $\gamma = 0.001$  (blue square), 0.005 (red circle), 0.01 (black up-triangle), 0.05 (magenta tilted square) and 0.1 (green tilted square). Similar to the RTPs shown in Fig. (6b), we observe  $\gamma D_{LH}(\rho, \gamma)$  is a decreasing function of density  $\rho$  and as one increases the inverse persistence length  $\gamma$ , it shows a crossover from  $1/\rho^2$  to  $1/\rho$ .

### B. Verification of the scaling form of gap distribution $P(g)$

In this section, we numerically verify the assumed exponential form of the gap distribution  $P(g)$  (see Eq. (8) and (9) in the main text)

$$P(g) \simeq N_* \exp(-g/g_*), \quad (28)$$

along with the following scaling relation satisfied by the typical gap size  $g_*$

$$g_* = \frac{1}{\rho} \mathcal{G}(\psi), \quad (29)$$

for the lattice gas model and RTPs. By using the conservation law  $\langle g \rangle = \sum_{g=1}^{\infty} g P(g) = 1/\rho$ , which is exact in the low density limit, we trivially obtain the proportionality constant

$$N_* = \frac{1}{\rho} \frac{[\exp(\rho/\mathcal{G}(\psi)) - 1]^2}{\exp(\rho/\mathcal{G}(\psi))}. \quad (30)$$

We now insert  $g_*$  and  $N_*$ , as shown in Eq. (29) and (30), in the expression of  $P(g)$ , defined in Eq. (28) and obtain the scaling relation for  $P(g)$ ,

$$-\ln\left(\frac{P(g)}{\rho}\right) = \frac{\rho g}{\mathcal{G}(\psi)} + 2 \ln(\mathcal{G}(\psi)). \quad (31)$$

Clearly the above scaling relation is a direct consequence of the assumed scaling form of  $g_*$ , which is shown in (29). Therefore the verification of Eq. (31) immediately yields the existence of the proposed scaling relation of  $g_*$ . In order to do that, we numerically obtain  $P(g)$  for RTPs (top panel) and lattice gas model (bottom panel) at various tumbling rates  $\gamma$  and densities  $\rho$ , such that

the ratio  $\psi = \rho/\gamma$  remains fixed. In Fig.(4), we plot  $-\ln(P(g)/\rho)$ , as a function of the scaled gap size  $\rho g$ , for two different  $\psi = 0.1$  and 0.5. For each  $\psi$ , we obtain data for three different tumbling rates  $\gamma = 0.05, 0.075$  and 0.1 and the corresponding density  $\rho$  are chosen from the relation  $\rho = \gamma\psi$ . As clearly evident from the figure, we observe data belonging in different parameter space

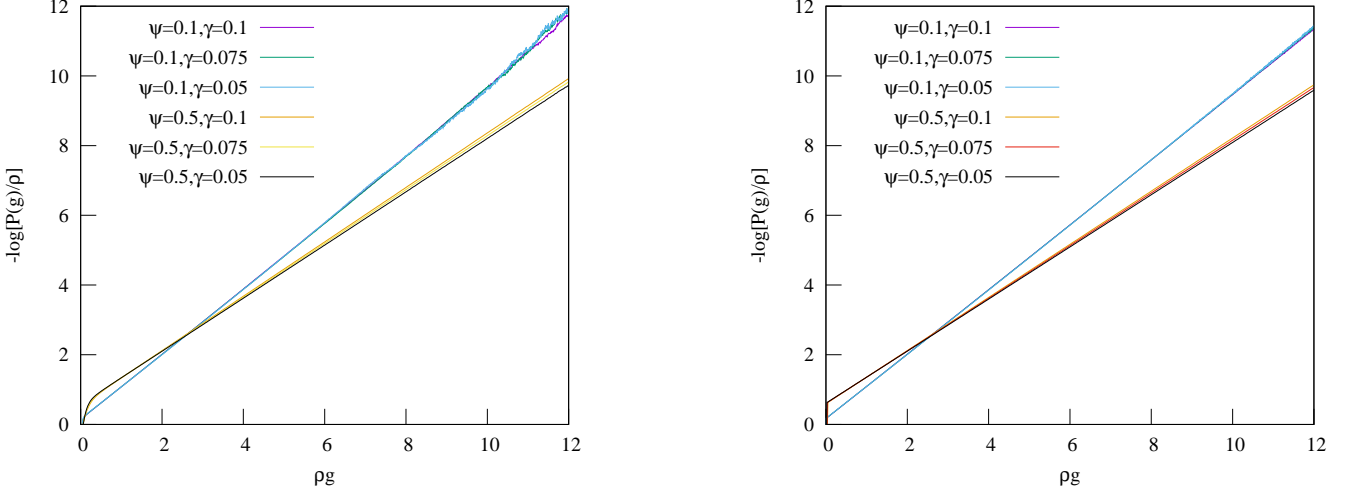


FIG. 4. Verification of Eq. (31). We plot  $-\ln(P(g)/\rho)$  as a function of  $\rho g$  for RTPs (left-panel) and lattice gas model (right-panel), for various combinations of  $\rho$  and  $\gamma$  such that the scaling variable  $\psi$  remains fixed at 0.1 and 0.5. In both these panels, for  $\psi = 0.1$ , we have used  $\gamma = 0.1$  (magenta line), 0.05 (green line) and 0.01 (sky blue line); while the same for  $\psi = 0.5$  are shown in orange line, black line and blue line respectively.

$(\rho, \gamma)$  corresponding to same  $\psi$  collapse with each other quite well, signalling the validity of the assumed form of  $g_*$  and the slope of the collapsed data is a measure of  $1/\mathcal{G}(\psi)$ .

### C. Derivation of scaling function $\mathcal{F}_{LH}(\psi)$ of the bulk-diffusion coefficient in the lattice gas

Here we derive the expression of the bulk-diffusivity  $\mathcal{D}_{LH}(\rho, \gamma)$  and the corresponding scaling function  $\mathcal{F}_{LH}(\psi)$ , displayed in the main text in Eq. (11). In the limit of small  $\gamma$  and  $\rho$ , we use the gap distribution function given in Eq. (28) and use it in Eq (6), and obtain

$$\mathcal{D}_{LH}(\rho, \gamma) = -\frac{1}{2} \frac{\partial}{\partial \rho} \left[ N_* \rho \sum_{l=1}^{\infty} \phi(l) \left( \sum_{g=1}^{\infty} g e^{-g/g_*} + (l-1) \sum_{g=l}^{\infty} (g-l) e^{-g/g_*} \right) \right]. \quad (32)$$

Now, using the following identities,

$$\sum_{g=1}^{\infty} g e^{-g/g_*} = \frac{e^{1/g_*}}{(e^{1/g_*} - 1)^2} = \frac{1}{N_* \rho}, \quad (33)$$

$$\sum_{g=l}^{\infty} (g-l) e^{-g/g_*} = \frac{e^{-(l-1)/g_*}}{(e^{1/g_*} - 1)^2} = \frac{e^{-l/g_*}}{N_* \rho}, \quad (34)$$

we can rewrite Eq. (32) in the following simplified way,

$$\mathcal{D}_{LH}(\rho, \gamma) = -\frac{\gamma}{2} \frac{\partial}{\partial \rho} \left[ \sum_{l=1}^{\infty} e^{-\gamma l} + \sum_{l=1}^{\infty} (l-1) e^{-(\gamma+1/g_*)l} \right] \quad (35)$$

Note that, the first term inside the square bracket of Eq. (35) is independent of  $\rho$  and vanishes upon differentiation. On the other hand, the summation appearing in the second term is given by,

$$\sum_{l=1}^{\infty} (l-1) e^{-(\gamma+1/g_*)l} = \frac{1}{(e^{(\gamma+1/g_*)} - 1)^2}. \quad (36)$$

We now use the scaling form of  $g_*$  as given in Eq. (29) and calculate,

$$\frac{\partial g_*}{\partial \rho} = -\frac{g_*}{\rho} \left( 1 - \psi \frac{\mathcal{G}'(\psi)}{\mathcal{G}(\psi)} \right). \quad (37)$$

Finally substituting all the results defined above in Eq. (35), the bulk-diffusion coefficient can be written as,

$$\mathcal{D}_{LH}(\rho, \gamma) = \frac{\gamma e^{(\gamma+\rho/\mathcal{G}(\psi))}}{\mathcal{G}(\psi) (e^{(\gamma+1/g_*)} - 1)^3} \left( 1 - \psi \frac{\mathcal{G}'(\psi)}{\mathcal{G}(\psi)} \right). \quad (38)$$

*Asymptotic expansion of  $\mathcal{D}_{LH}(\rho, \gamma)$ :* We can further expand the bulk-diffusion coefficient  $\mathcal{D}_{LH}(\rho, \gamma)$ , obtained



in Eq. (38), in the limit of  $\gamma \rightarrow 0$  and  $\rho \rightarrow 0$ , such that the dimensionless quantity  $\psi = \rho/\gamma$  remains finite. Let us first make the replacement,

$$n = \gamma + \frac{1}{g_*} = \gamma + \frac{\rho}{\mathcal{G}(\psi)} \equiv \gamma \left( 1 + \frac{\psi}{\mathcal{G}(\psi)} \right). \quad (39)$$

Note that this particular limit of interest automatically implies  $n \rightarrow 0$ . We now expand,

$$\begin{aligned} \frac{\gamma e^n}{(e^n - 1)^3} &= \frac{\gamma (1 + n + n^2 \dots)}{n^3 \left( 1 + \frac{n}{2} + \frac{n^2}{6} \dots \right)^3} \\ &\simeq \gamma \left( \frac{1}{n^3} - \frac{1}{2n^2} - \frac{3}{2n} \dots \right). \end{aligned} \quad (40)$$

Since we are working in the regime  $n \rightarrow 0$ , the leading order contribution to Eq. (40) emerges from  $1/n^3$  term only and consequently the bulk-diffusion coefficient can be written as

$$\begin{aligned} \mathcal{D}_{LH}(\rho, \gamma) &= \frac{\gamma}{n^3 \mathcal{G}(\psi)} \left( 1 - \psi \frac{\mathcal{G}'(\psi)}{\mathcal{G}(\psi)} \right) + \mathcal{O} \left( \frac{\gamma}{n^2} \right), \\ &\simeq \frac{\mathcal{G}^2(\psi)}{\gamma^2 (\mathcal{G}(\psi) + \psi)^3} \left( 1 - \psi \frac{\mathcal{G}'(\psi)}{\mathcal{G}(\psi)} \right) + \mathcal{O} \left( \frac{1}{\gamma} \right). \end{aligned} \quad (41)$$

From the above equation, it is quite evident that  $\mathcal{D}_{LH}(\rho, \gamma)$  satisfies a scaling relation and the corresponding scaling function can be written as

$$\mathcal{F}_{LH}(\rho, \gamma) = \gamma^2 \mathcal{D}_{LH}(\rho, \gamma) \simeq \frac{\mathcal{G}^2(\psi)}{(\mathcal{G}(\psi) + \psi)^3} \left( 1 - \psi \frac{\mathcal{G}'(\psi)}{\mathcal{G}(\psi)} \right). \quad (42)$$

#### D. Numerical scheme to calculate the bulk-diffusion coefficients for Run-and-Tumble particles (RTPs)

Due to non-trivial spatio-temporal correlations and non-gradient property at the microscopic scale, we could not proceed through the above mentioned analytic calculations which leads us to adopt a numerical scheme, mentioned in [40], to calculate the absolute bulk-diffusion coefficient  $D_{RTP}(\rho, \gamma)$ , which is related with the scaled bulk-diffusion coefficient as  $\mathcal{D}_{RTP}(\rho, \gamma) = D_{RTP}(\rho, \gamma)/\gamma$ . According to the scheme, in response to a slowly varying initial sinusoidal perturbation shown in Eq. (43), the system tries to attain a stationary state and the long wavelength relaxation rate directly measures the bulk-diffusivity of the system. In this analysis, we let the system evolve from an initial density perturbation,

$$\delta\rho(x, 0) = \rho(x, 0) - \rho_0 = A(0) \sin(2\pi x), \quad (43)$$

where  $\rho_0$  is the uniform background density over which the perturbation is applied. On the coarse-grained scale i.e.  $x = X/L$  and  $\tau = t/L^2$  (here  $t$  is unscaled microscopic time for RTPs), the system is assumed to overcome

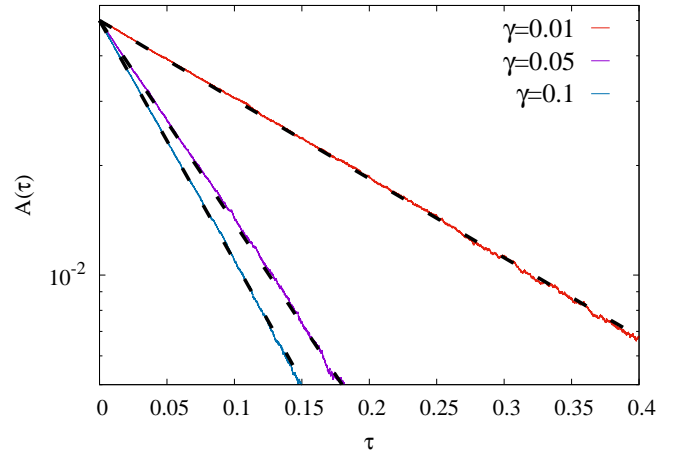


FIG. 5. We have plotted perturbation amplitude  $A(\tau)$ , as a function of the hydrodynamic time  $\tau$ , for tumbling rates  $\gamma = 0.01$  (red line),  $0.05$  (magenta line) and  $0.1$  (blue line), while the black dotted lines are the best fitted data, which according to Eq. (47), we obtain relaxation rates  $\Gamma = 5, 12.8$  and  $15.2$  for  $\gamma = 0.01, 0.05$  and  $0.1$  respectively. For both these panels, we have fixed  $\rho = 0.5$  and  $A(0) = \rho_0/10 = 0.05$ .

the ballistic relaxation mode due to inherent persistence (we verify this in sec.) and consequently the density field  $\rho(x, \tau)$  evolves according to the diffusion equation,

$$\frac{\partial \rho(x, \tau)}{\partial \tau} = \frac{\partial}{\partial x} \left[ D(\rho, \gamma) \frac{\partial \rho(x, \tau)}{\partial x} \right]. \quad (44)$$

which in general is a nonlinear equation and is difficult to solve exactly for arbitrary  $\tau$ . However, in the limit of small perturbation, i.e.  $A(0) \ll \rho_0$ , we can write  $D[\rho(x, \tau)] \simeq D(\rho_0)$  and consequently Eq. (44) becomes linear, i.e.

$$\frac{\partial \rho(x, \tau)}{\partial \tau} = D(\rho_0, \gamma) \frac{\partial^2 \rho(x, \tau)}{\partial x^2}, \quad (45)$$

which admits the following solution,

$$\delta\rho(x, \tau) = \rho(x, \tau) - \rho_0 = A(\tau) \sin(2\pi x). \quad (46)$$

Here the amplitude  $A(\tau)$  is given by,

$$A(\tau) = A(0) e^{-4\pi^2 D_{RTP}(\rho_0) \tau} \equiv A(0) e^{-\Gamma(\rho_0) \tau} \quad (47)$$

and the relaxation rate is given by,

$$\Gamma(\rho, \gamma) = 4\pi^2 D_{RTP}(\rho, \gamma). \quad (48)$$

Note that, the relaxation rate  $\Gamma$  is a function of density  $\rho$  as well as the tumbling rate  $\gamma$ . In simulations, we measure  $\Gamma$  and use Eq. (48) to obtain the bulk-diffusion coefficient  $D_{RTP}(\rho, \gamma)$  of the system. As the characterization of collective diffusion is the focal point of our work, we require the system to reach the diffusive regime. We

ensure this by evolving the system upto  $t \sim L^2$ , where  $L$  is large implying the relaxation of long wavelength mode. In this process, we take the system size limit  $L \gg 1$  first and then varying the tumbling rate  $\gamma$  carefully, so that the typical persistent length  $l_p = \gamma^{-1}$  always remains much smaller than  $L$ , i.e.  $l_p \ll L$ . We typically choose the system size upto  $L = 3000$ . For example, at the top panels of Fig. 5, we have shown density profiles, as a function of scaled position  $x$ , at various hydrodynamic times  $\tau = 0.01$  (blue circles), 0.02 (black up-triangle) and 0.1 (magenta down-triangle) for tumbling rate  $\gamma = 0.01$  (left panel) and 0.05 (right panel) respectively; while at the bottom panel, we have plotted the time variation of the perturbation amplitude  $A(\tau)$ , which indeed shows exponential decay as in Eq. (47). Calculating the slope of decay in semi-log scale, the relaxation decay is estimated, which according to Eq. (48), gives the bulk-diffusion coefficient  $D(\rho, \gamma)$  of the system.

In Fig. (6a) we plot the absolute bulk-diffusion coefficient  $D_{RTP}(\rho, \gamma)$  as a function of tumbling rate  $\gamma$  at various densities  $\rho = 0.01$  (blue square), 0.05 (red circle), 0.1 (black upper-triangle), 0.5 (magenta lower-triangle). At large  $\gamma$ , we observe  $D_{RTP}(\rho, \gamma)$  to be independent of both  $\rho$  and  $\gamma$  and approaches to a constant value  $1/2$  which is expected, as in this limit, particles randomly flip their orientation and the RTP dynamics essentially transforms into the well known symmetric simple exclusion process (SSEP) in which case the diffusion coefficient is indeed  $1/2$  at all densities. On the other hand, at small  $\gamma$ , particles tend to move persistently along the same direction for a long time which enhances diffusion. However, the free propagation of persistently moving particles gets obstructed by the presence of other particles due to hard-core repulsion, which restricts particles to diffuse. Therefore, persistence and hard-core repulsion act in the opposite sense and the interplay between them essentially leads to nonmonotonic variation of bulk-diffusion coefficient  $D_{RTP}(\rho, \gamma)$  in tumbling rate  $\gamma$ . When the interparticle spacing  $\rho^{-1}$  is larger than the persistent length  $\gamma^{-1}$ , particles barely feel the presence of others and the persistence effect dominates over hard-core repulsion, which in turn increases the bulk-diffusion coefficient  $D_{RTP}(\rho, \gamma)$  with decreasing  $\gamma$ . Keeping  $\rho$  fixed at a finite value, when one decreases  $\gamma$  further and reaches the opposite limit i.e.  $\rho^{-1} < \gamma^{-1}$ , the hardcore repulsion dominates over persistence and two oppositely moving particles upon collision block each other's movement. Since spin flipping time is quite large in this limit, by the time one of them reorient its direction to restart their journey, many other particles approach them from both the directions and eventually particles are trapped inside a cluster with two boundary particles orienting themselves towards the cluster, which significantly reduces  $D_{RTP}(\rho, \gamma)$  of the system. In such case, diffusion takes place only when one of the boundary particles from a cluster flips and, as we know local spin-flipping event takes place at a time scale  $1/\gamma$ , we expect the bulk-diffusion coefficient  $D_{RTP}(\rho, \gamma) \sim \gamma$  for very small tumbling rate  $\gamma$ . Fig. (6b) we show the varia-

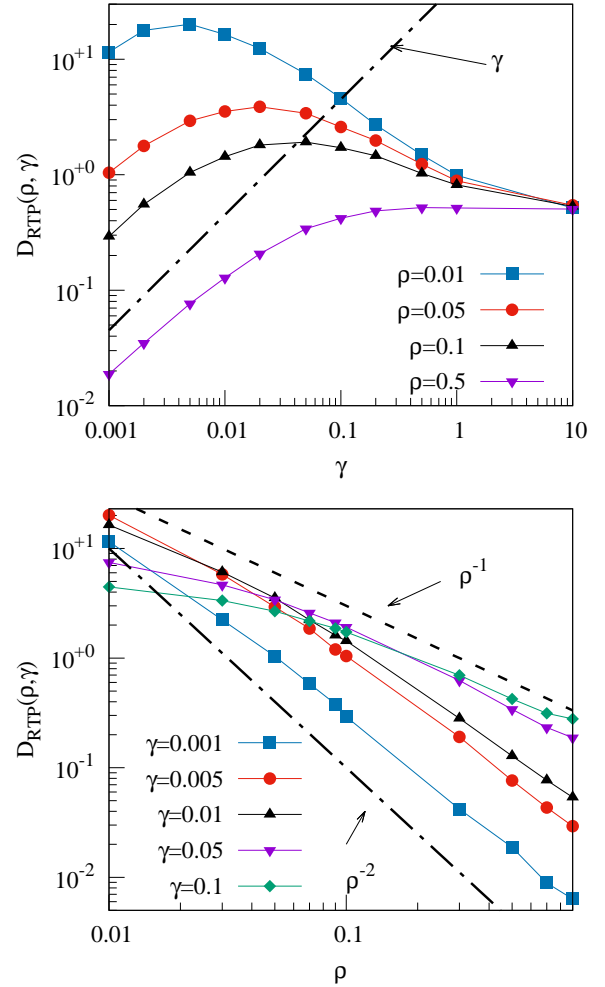


FIG. 6. Bulk-diffusion coefficient for run-and-tumble particles. In the left panel, we plot  $D(\rho, \gamma)$  as a function of spin-flipping rate  $\gamma$  for various density  $\rho = 0.01$  (blue square), 0.05 (red circle), 0.1 (black up-triangle), 0.5 (magenta down-triangle), while in the right panel,  $D(\rho, \gamma)$  is plotted against density  $\rho$  for different spin-flipping rate  $\gamma = 0.001$  (blue square), 0.005 (red circle), 0.01 (black up-triangle), 0.05 (magenta down-triangle) and 0.1 (green tilted square).

tion of  $D(\rho, \gamma)$  with  $\rho$  at different  $\gamma = 0.001$  (blue square), 0.005 (red circle), 0.01 (black upper-triangle), 0.05 (magenta lower-triangle) and 0.1 (green tilted-square). Unlike Fig. (6a), in this case  $D_{RTP}(\rho, \gamma)$  is observed to be a monotonically decreasing function of  $\rho$ . For a fixed  $\gamma$ , as one increases  $\rho$ , the typical interparticle spacing is reduced and hence hard-core repulsion effect dominates over persistent motion of particles and as before  $D_{RTP}(\rho, \gamma)$  decreases.

### E. Verification of the existence of diffusive scaling limit for RTPs

One of the central assumptions in calculating  $D_{RTP}(\rho, \gamma)$  is that the long wavelength relaxation is only dominated by the diffusive modes and consequently the time evolution of the density field  $n(X, t)$  can be described by the diffusion equation, i.e., on a coarse-grained scale the system should satisfy diffusive scaling:  $n(X, t) = \rho(X/L, t/L^2)$ ,  $J(X, t) = L^{-1}j(X/L, t/L^2)$ . Here we want to verify the existence of such scaling for RTPs. For this purpose, we study the relaxation of the density field  $\rho(x, \tau)$  as a function of scaled position  $x = X/L$  for different system sizes  $L$  and different microscopic times  $t$  such that the hydrodynamic time  $\tau = t/L^2$  remains fixed. The scaling limit would be verified if different curves corresponding to different  $L$  at the same  $\tau$  collapse with each other and the collapsed data must be the solution of the nonlinear diffusion equation Eq. (44).

To verify the diffusive scaling limit, we simulate the model with a slowly varying sinusoidal density profile over a uniform background as defined in Eq. (43). In Fig. (E), we plot the scaled excess density field  $\delta\rho(x, \tau) = \rho(x, \tau) - \rho_0$ , obtained from simulation, as a function of the scaled position  $x = X/L$  for different system sizes  $L = 1000$  (blue square),  $2000$  (magenta triangle) and  $3000$  (red circle) at  $\gamma = 0.01$  and  $0.005$  respectively, while the hydrodynamic time and the density are fixed at  $\tau = 0.2$  and  $\rho_0 = 0.5$ . We also numerically integrate Eq. (44) using the initial condition defined in Eq. (43) and the corresponding solution is plotted in black solid line. We observe the simulation points along with the analytic solution collapse quite well and hereby assert the existence of diffusive scaling limit for RTPs.

### F. Verification of hydrodynamics through density relaxation

In this section, we further verify the hydrodynamic description Eq. (44) by relaxing the initial density perturbation through the already obtained bulk-diffusion coefficients  $D_{RTP}(\rho, \gamma)$  and  $D_{LH}(\rho, \gamma)$  for RTPs and the lattice gas respectively. As mentioned above, on the coarse grained scale, i.e.,  $x = X/L$  and  $\tau = t/L^2$ , the density relaxation is governed by the non-linear diffusion equation Eq. (44) and we can compare the exact numerical solution of Eq. (44) (obtained through Euler integration method) and compare with simulations. For this purpose, we take the initial density perturbation to be a step-function with step height  $\rho_1$  and width  $w$  over a uniform background density  $\rho_0$ , which mathematically can be expressed as,

$$\rho(x, \tau = 0) = \begin{cases} \rho_0 + \rho_1 & \text{for } |x - \frac{1}{2}| \leq \frac{w}{2}, \\ \rho_0 & \text{otherwise.} \end{cases} \quad (49)$$

In Fig. 8 we plot the excess density field  $\delta\rho(x, \tau) = \rho(x, \tau) - \rho_0$ , obtained from simulation, as a function of the coarse-grained space  $x = X/L$  using the initial condition

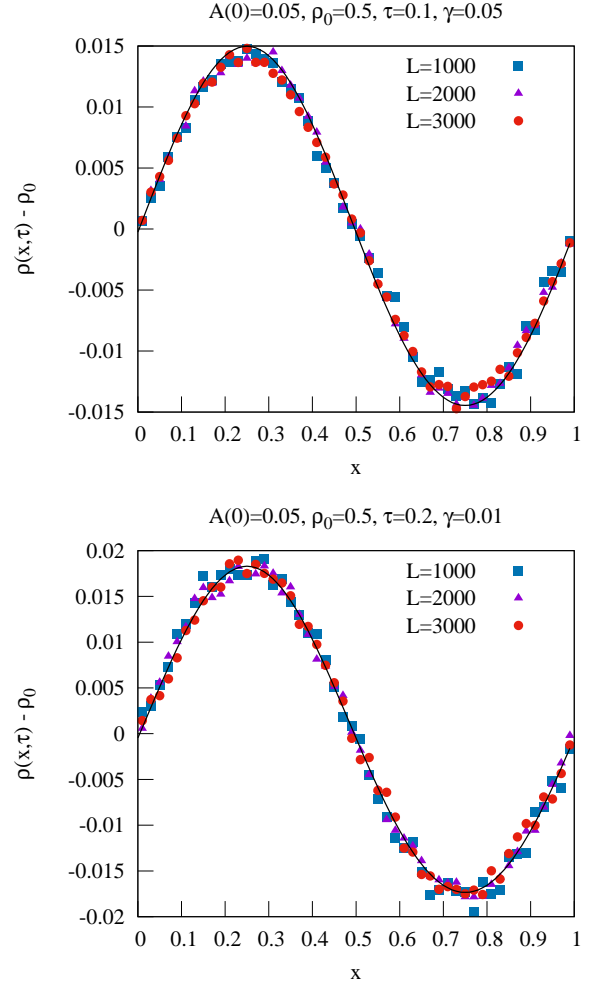


FIG. 7. *Verification of diffusive scaling.* In the left panel, we plot the excess density field  $\delta\rho(x, \tau) = \rho(x, \tau) - \rho_0$  for  $\gamma = 0.05$ , obtained from simulation, as a function of the scaled position  $x = X/L$  at different microscopic times  $t = 1 \times 10^5$  for  $L = 1000$  (blue square),  $t = 4 \times 10^5$  for  $L = 2000$  (magenta up-triangle) and  $t = 9 \times 10^5$  for  $L = 3000$  (red circle) such that the hydrodynamic time is fixed at  $\tau = t/L^2 = 0.1$ , while in the right panel, we plot the same for  $\gamma = 0.01$  at  $t = 2 \times 10^5$  for  $L = 1000$  (blue square),  $t = 8 \times 10^5$  for  $L = 2000$  (magenta up-triangle) and  $t = 1.8 \times 10^6$  for  $L = 3000$  (red circle) such that the hydrodynamic time is fixed at  $\tau = t/L^2 = 0.2$ . In both the cases we relax the system with a sinusoidally varying initial condition defined in Eq. (43) with  $\rho_0 = 0.5$ . Corresponding lines are obtained by numerically integrating the hydrodynamic equation using the bulk-diffusion coefficient obtained from simulation. For both the  $\gamma$  values, density profiles corresponding to same  $\tau$  for different  $L$  collapse quite well.

defined in Eq. (49) at different hydrodynamic times  $\tau = 10^{-3}$  (red tilted-square),  $2 \times 10^{-3}$  (black up-triangle),  $5 \times 10^{-3}$  (magenta down-triangle) and the corresponding lines are obtained by numerically integrating Eq. (44) using our obtained diffusion coefficient  $\mathcal{D}_{RTP}(\rho, \gamma)$  with the same initial condition defined in Eq. (49). The result

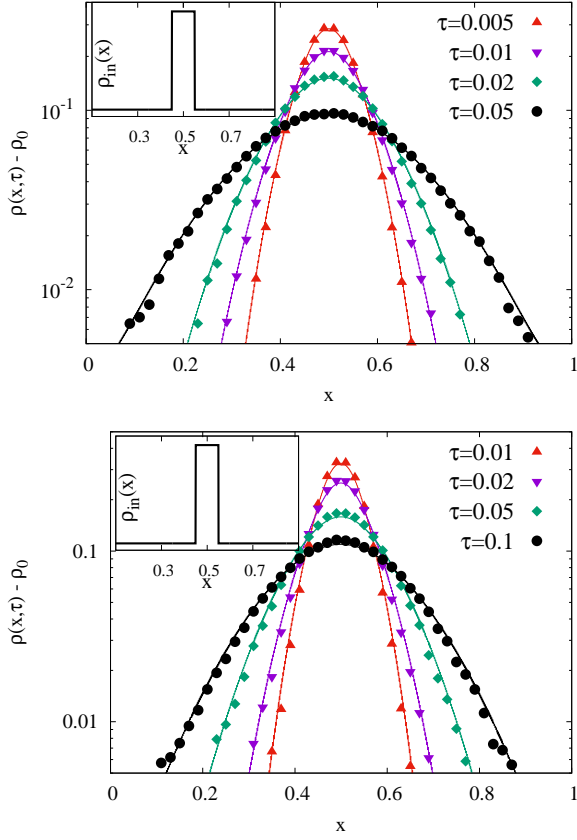


FIG. 8. *Verification of bulk-diffusion coefficient  $D_{RTP}(\rho, \gamma)$ .* We verify the bulk-diffusion coefficient  $D_{RTP}(\rho, \gamma)$  through the relaxation from an initial density perturbation, defined in Eq. (49), at various hydrodynamic times  $\tau$ . In the top panel, we plot the numerically obtained excess density profile  $\delta\rho(x, \tau) = \rho(x, \tau) - \rho_0$  for  $\gamma = 0.05$  as a function of the scaled position  $x$  at  $\tau = 0.005$  (red up-triangle), 0.01 (magenta down-triangle), 0.02 (green tilted square) and 0.05 (black circle). In the bottom panel we plot the same for  $\gamma = 0.01$  at  $\tau = 0.01$  (red up-triangle), 0.02 (magenta down-triangle), 0.05 (green tilted square) and 0.1 (black circle). Corresponding lines are the data obtained by integrating the hydrodynamic equation. For both the cases, we relax the system from same initial condition with  $\rho_0 = 0.5$ ,  $\rho_1 = 0.4$  and  $w = 0.1$  and they are plotted at the inset of the respective panels.

is obtained for  $\gamma = 0.05$ ,  $L = 1000$ ,  $\rho_1 = 0.4$ ,  $\rho_0 = 0.5$  and  $w = 0.1$ . The simulation data matches quite well with the hydrodynamic theory, therefore the obtained diffusion coefficient  $D_{RTP}(\rho, \gamma)$  is correct.

For the lattice gas model we proceed with  $\rho_0 = 0.5$ ,  $\rho_1 = 0.4$ ,  $w = 0.1$  and the relaxation is studied for two different  $\gamma = 0.05$  and 0.01, same as RTPs. In the left panel of Fig. 9, we plot the excess density field  $\delta\rho(x, \tau)$ , obtained from simulations, as a function of the scaled position  $x$  for  $\gamma = 0.05$  at different hydrodynamic time  $\tau = 0.001$  (blue square), 0.002 (red circle), 0.005 (black up-triangle), 0.01 (magenta down-triangle), while at the right panel, we plot the same for  $\gamma = 0.01$  at  $\tau = 0.002$

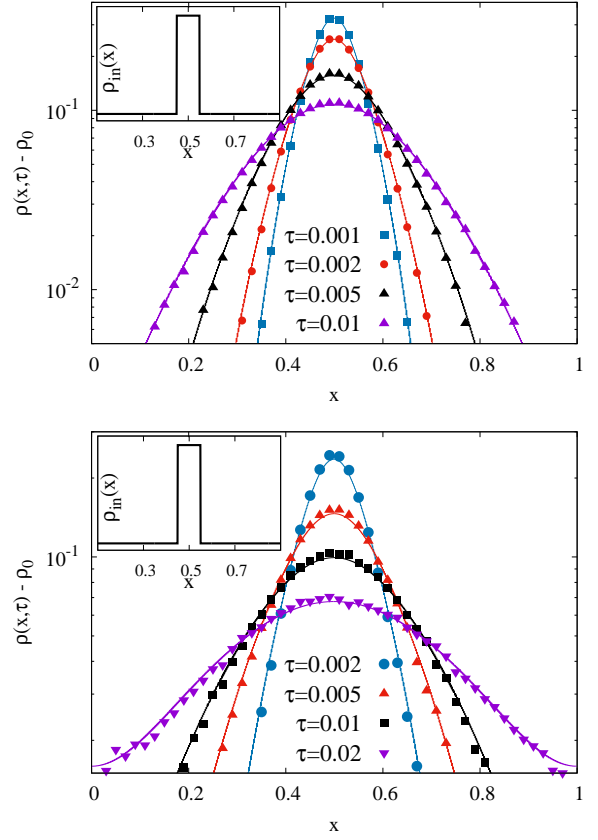


FIG. 9. *Verification of bulk-diffusion coefficient  $D_{LH}(\rho, \gamma)$ .* We verify the bulk-diffusion coefficient  $D_{LH}(\rho, \gamma)$  through the relaxation from an initial density perturbation, defined in Eq. (49), at various hydrodynamic times  $\tau$ . In the top panel, we plot the numerically obtained excess density profile  $\delta\rho(x, \tau) = \rho(x, \tau) - \rho_0$  for  $\gamma = 0.05$  as a function of the scaled position  $x$  at  $\tau = 0.001$  (blue square), 0.002 (red circle), 0.005 (black up-triangle) and 0.01 (magenta down-triangle). In the bottom panel, we plot the same for  $\gamma = 0.01$  at  $\tau = 0.002$  (blue circle), 0.005 (red up-triangle), 0.01 (black square) and 0.02 (magenta down triangle). Corresponding lines are the data obtained by integrating the hydrodynamic equation. For both the cases, we relax the system from same initial condition with  $\rho_0 = 0.5$ ,  $\rho_1 = 0.4$  and  $w = 0.1$  and they are plotted at the inset of the respective panels.

(blue circle), 0.005 (red up-triangle), 0.01 (black square), 0.02 (magenta down-triangle). To verify the hydrodynamic density evolution equation or the obtained bulk diffusion coefficient  $\mathcal{D}_{LH}(\rho, \gamma)$ , we perform Euler integration of Eq. (44) by using the initial condition defined in Eq. (49) for the same parameters defined above and plot the solutions as lines in both the panels of Fig. 9. For both the  $\gamma$  values, we observe a good match between the simulation data (points) and hydrodynamic theory (line).

### G. Verification of emergent hydrodynamics

As discussed in the main text, in the limit of strong persistence i.e.  $\gamma \rightarrow 0$ , the unscaled bulk-diffusion coefficient  $D_{RTP}(\rho, \gamma)$  shows anomalous behavior; in the low density limit, it diverges as  $1/\gamma$ , while in the finite density limit, it vanishes as  $D_{RTP} \sim \gamma$ . Furthermore, on the time scale of RTPs, the bulk-diffusion coefficient of the lattice gas model  $\gamma D_{LH}(\rho, \gamma)$ , exhibits similar characteristics. Consequently, the hydrodynamic description is not meaningful in the limit  $\gamma \rightarrow 0$ . Therefore, to maintain an appropriate hydrodynamic structure, one cannot independently vary  $\rho$  and  $\gamma$  and, from the scaling relation satisfied by  $\mathcal{D}(\rho, \gamma)$ , we see that proper hydrodynamics scaling is recovered only when we rescale the density field  $\psi = \rho/\gamma$  and time  $\tilde{\tau} = \tau/\gamma^2$  and the corresponding hydrodynamic equation is given by,

$$\frac{\partial \psi(x, \tilde{\tau})}{\partial \tilde{\tau}} = \frac{\partial}{\partial x} \left[ \mathcal{F}(\psi) \frac{\partial \psi(x, \tilde{\tau})}{\partial x} \right]. \quad (50)$$

To verify Eq. (50) for RTPs and lattice gas, in Fig. (10) we plot the scaled density field  $\psi(x, \tilde{\tau}) = \rho(x, \tau = \tilde{\tau}\gamma)/\gamma$  as a function of coarse-grained position  $x = X/L$  for different spin-flipping rate  $\gamma$  and hydrodynamic time  $\tau$  while keeping the rescaled time  $\tilde{\tau} = \tau/\gamma$  fixed. Different curves corresponding to different  $\gamma$  at the same  $\tilde{\tau}$  are expected to collapse with each other and the collapsed profile at different  $\tilde{\tau}$  should be governed by the solution of the nonlinear diffusion equation Eq. (50). We choose the initial scaled density profile  $\psi(x, \tilde{\tau} = 0)$  to be a step function with step height  $\psi_1$  and width  $w$  over a uniform background profile  $\psi_0$ , i.e.

$$\psi(x, \tilde{\tau} = 0) = \begin{cases} \psi_0 + \psi_1 & \text{for } |x - \frac{1}{2}| \leq \frac{w}{2}, \\ \psi_0 & \text{otherwise.} \end{cases} \quad (51)$$

For a fixed  $\gamma$ , we prepare a step profile for the density field  $n(X, 0)$  with step height  $\rho_1$  and width  $w$  around  $x = 1/2$  over a uniform background density  $\rho_0$  such that the rescaled density  $\psi_0 = \rho_0/\gamma$  and  $\psi_1 = \rho_1/\gamma$  remain fixed for all  $\gamma$ . In Fig. 10a and 10b, for a fixed  $\psi_0 = 40$  and  $\psi_1 = 40$  we plot the relaxation of the excess rescaled density field  $\psi(x, \tilde{\tau}) - \psi_0$ , obtained from simulation, as a function of  $x$  for different  $\gamma = 0.01$  (open symbols) and  $0.005$  (closed symbols) at various rescaled hydrodynamic time  $\tilde{\tau} = 5$  (red line),  $10$  (blue line) and  $20$  (magenta line) for RTPs and  $\tilde{\tau} = 40$  (red line),  $80$  (blue line) and  $160$  (magenta line) for lattice gas respectively and the corresponding lines are the results from numerical integration of Eq. (50) with the same initial condition using numerically obtained  $\mathcal{F}_{RTP}(\psi)$  for RTPs and  $\mathcal{F}_{LH}(\psi)$  for lattice gas as given in Eq. (12) in the main text. Simulation and analytical data corresponding to these two different  $\gamma$  values are observed to collapse quite well for both these models, which consequently verifies the existence of the proper hydrodynamic equation Eq. (50).

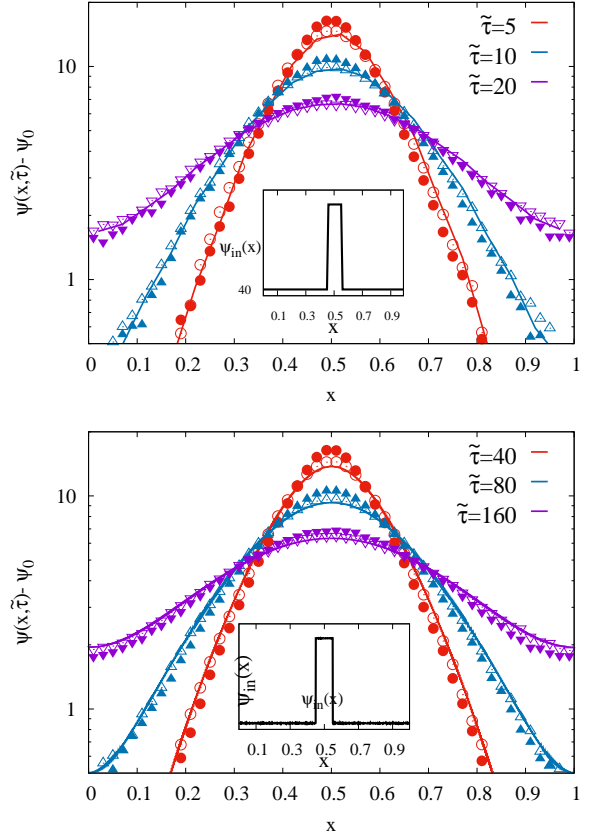


FIG. 10. *Relaxation of scaled density field  $\psi(x, \tilde{\tau})$ .* We plot the scaled excess density field  $\delta\psi(x, \tilde{\tau}) = \psi(x, \tilde{\tau}) - \psi_0$ , for RTPs (top-panel) and the lattice gas model (bottom-panel), as a function of the scaled position  $x$  at various rescaled time  $\tilde{\tau}$  for two different  $\gamma = 0.005$  and  $0.01$ . In case of RTPs, for  $\gamma = 0.005$ , we numerically obtain excess density profiles  $\delta n(X, \tau)$  with  $\rho_0 = 0.2$ ,  $\rho_1 = 0.2$  at hydrodynamic times  $\tau = 1.25 \times 10^{-4}$  (red filled circle),  $2.5 \times 10^{-4}$  (blue filled up-triangle),  $5 \times 10^{-4}$  (magenta filled down-triangle) (for RTPs) and  $\tau = 10^{-3}$  (red filled circle),  $2 \times 10^{-3}$  (blue filled up-triangle),  $4 \times 10^{-3}$  (magenta filled down-triangle) (for lattice gas model); while the corresponding parameters for  $\gamma = 0.01$  are  $\rho_0 = 0.4$ ,  $\rho_1 = 0.4$ ,  $\tau = 5 \times 10^{-4}$  (red open circle),  $10 \times 10^{-4}$  (blue open up-triangle),  $20 \times 10^{-4}$  (magenta open down-triangle) (for RTPs) and  $\tau = 4 \times 10^{-3}$  (red open circle),  $8 \times 10^{-3}$  (blue open up-triangle),  $1.6 \times 10^{-2}$  (magenta open down-triangle) (for lattice gas) such that the rescaled variables are fixed at  $\psi_0 = \rho_0/\gamma = 40$ ,  $\psi_1 = \rho_1/\gamma = 40$  and  $\tilde{\tau} = \tau/\gamma^2 = 5, 10, 20$  (for RTPs) and  $40, 80, 160$  (for lattice gas). Corresponding lines are obtained by integrating Eq. (50) using the scaling function  $\mathcal{F}_{RTP}(\psi)$  obtained from simulation and  $\mathcal{F}_{LH}(\psi)$  from Eq. (12) in main text. We observe a good collapse between simulation points and theoretical lines.

### H. Power-law dependence of the bulk-diffusion coefficient

In the main text, we have characterized the ballistic transport of active particles for tumbling rate  $\gamma = 0.05$ . The scaling relation is obtained by assuming the  $1/\rho$  de-



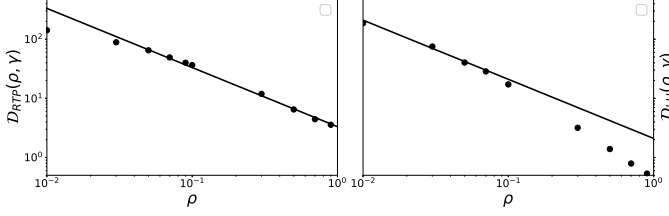


FIG. 11. We plot the scaled bulk-diffusion coefficients  $\mathcal{D}_{RTP}(\rho, \gamma)$  and  $\mathcal{D}_{LH}(\rho, \gamma)$  as a function of  $\rho$  for RTPs (left-panel) and lattice gas (right-panel), respectively; guiding lines represent the power-law form  $C/\rho$  which was used to derive the scaling function  $\mathcal{R}(\xi)$  in Eq. (14) and where the values of  $C$  depend on the microscopic details of the model -  $C = 3.32$  for RTPs and  $C = 2.2$  for lattice gas model respectively. Here note that, for RTPs the scaled bulk-diffusion coefficient is  $\mathcal{D}_{RTP} \equiv D_{RTP}/\gamma$  and for lattice gas  $\mathcal{D}_{LH} \equiv D_{LH}$ .

pendence of the bulk-diffusion coefficient  $\mathcal{D}(\rho, \gamma)$ . To support this assumption, in Fig. 11, we present the density dependence of the numerically obtained  $\mathcal{D}(\rho, \gamma)$  for RTPs (left-panel) and the lattice gas model (right-panel). We observe over a broad range in density,  $\mathcal{D}(\rho, \gamma)$  obeys  $1/\rho$  scaling which is shown here by the solid black line.

### I. Calculation of the scaling function $\mathcal{R}(\xi)$

In this section, we will show quantitatively how power-law density dependence in bulk-diffusion coefficient leads to anomalous scaling in collective transport, as discussed in the main text. For this purpose, the most general expression of the bulk-diffusion coefficient can be written as

$$\mathcal{D}(n) \simeq \frac{C}{n^\alpha}, \quad (52)$$

where the coefficient  $C$  and the exponent  $\alpha$  depend on the specific model considered. The corresponding evolution equation of the microscopic density  $n(X, t)$  is given by,

$$\frac{\partial n(X, t)}{\partial t} = C \frac{\partial}{\partial X} \left( \frac{1}{n^\alpha} \frac{\partial n}{\partial X} \right), \quad (53)$$

where  $X$  and  $t$  are the space and time coordinates, respectively, at the microscopic scale. In order to solve the above equation, from an initially localized distribution  $n(X, 0) = n_1 \delta(X)$ , we proceed with the following scaling

ansatz,

$$n(X, t) = \frac{1}{(Ct)^\omega} \mathcal{R} \left( \frac{X}{(Ct)^\omega} \right), \quad (54)$$

where  $\xi = X/(Ct)^\omega$  is the scaling variable. Note that, the growth exponent  $\omega$  essentially characterizes the anomaly in the collective transport;  $\omega = 1/2$  corresponds to normal diffusive transport, while  $\omega > 1/2$  and  $\omega < 1/2$  indicate the transport to be superdiffusive and subdiffusive respectively. Finally plugging the above scaling solution in Eq. (53), we obtain

$$\omega \frac{d(\xi \mathcal{R})}{d\xi} = -(Ct)^{1-(2-\alpha)\omega} \frac{d}{d\xi} \left[ \mathcal{R}^{-\alpha} \frac{d\mathcal{R}}{d\xi} \right]. \quad (55)$$

However, to exhibit self-similar solution, Eq. (55) should not contain  $t$  explicitly, implying  $1 - (2 - \alpha)\omega = 0$ , or

$$\omega = \frac{1}{2 - \alpha}. \quad (56)$$

Eq. (56) directly relates the growth exponent  $\omega$  to the exponent  $\alpha$  and is displayed in the main text.

We note that, depending on the parameter regime the exponent  $\alpha$  lies in the range  $0 \leq \alpha \leq 2$ . Now, to demonstrate Eq. (53) and Eq. (55), we choose a particularly interesting regime for which  $\alpha = 1$  and, from Eq. (56), it immediately implies  $\omega = 1$ . This indicates the model should exhibit *ballistic* transport. In this particular regime,  $\mathcal{R}(\xi)$  obeys the following equation,

$$\frac{d(\xi \mathcal{R})}{d\xi} = -\frac{d^2}{d\xi^2} [\ln \mathcal{R}]. \quad (57)$$

By using the boundary condition  $d\mathcal{R}/d\xi = 0$  for  $\xi = 0$  (source free solution), the above equation reduces to

$$\frac{d \ln \mathcal{R}}{d\xi} = -\xi \mathcal{R}. \quad (58)$$

We further use another boundary condition  $\mathcal{R}(\xi = 0) = \xi_0^2/2$ , which immediately implies the solution to be,

$$\mathcal{R}(\xi) = \frac{2}{\xi_0^2 + \xi^2}. \quad (59)$$

The above solution is the desired scaling function which we display in the main text in Eq. (14).

- 
- [1] M. C. Marchetti, J. F. Joanny, S. Ramaswamy, T. B. Liverpool, J. Prost, M. Rao, and R. A. Simha, *Rev. Mod. Phys.* **85**, 1143 (2013).  
[2] B. Wang, S. M. Anthony, S. C. Bae, and S. Granick, *Proceedings of the National Academy of Sciences* **106**, 15160 (2009). <https://www.pnas.org/doi/pdf/10.1073/pnas.0903554106>.  
[3] K. C. Leptos, J. S. Guasto, J. P. Gollub, A. I. Pesci, and R. E. Goldstein, *Phys. Rev. Lett.* **103**, 198103 (2009).  
[4] B. Wang, J. Kuo, S. C. Bae, and S. Granick, *Nature Materials* **11**, 481 (2012).  
[5] Ariel, A. Rabani, S. Benisty, J. D. Partridge, R. M. Harshey, and A. Be'Er, *Nature communications* **6**, 1

- (2015).
- [6] H. M. López, J. Gachelin, C. Douarche, H. Auradou, and E. Clément, *Phys. Rev. Lett.* **115**, 028301 (2015).
- [7] A. Sokolov, L. D. Rubio, J. F. Brady, and I. S. Aranson, *Nature communications* **9**, 1 (2018).
- [8] A. G. Cherstvy, O. Nagel, C. Beta, and R. Metzler, *Physical Chemistry Chemical Physics* **20**, 23034 (2018).
- [9] A. Lagarde, N. Dagès, T. Nemoto, V. Démery, D. Bartolo, and T. Gibaud, *Soft Matter* **16**, 7503 (2020).
- [10] P. T. Underhill, J. P. Hernandez-Ortiz, and M. D. Graham, *Phys. Rev. Lett.* **100**, 248101 (2008).
- [11] Z. Liao, M. Han, M. Fruchart, V. Vitelli, and S. Vaikuntanathan, *The Journal of chemical physics* **151**, 194108 (2019).
- [12] Y. Hatwalne, S. Ramaswamy, M. Rao, and R. A. Simha, *Phys. Rev. Lett.* **92**, 118101 (2004).
- [13] S. Belan and M. Kardar, *The Journal of Chemical Physics* **150**, 064907 (2019).
- [14] A. R. Dulaney and J. F. Brady, *Phys. Rev. E* **101**, 052609 (2020).
- [15] P. Le Doussal, S. N. Majumdar, and G. Schehr, *EPL (Europhysics Letters)* **130**, 40002 (2020).
- [16] S. C. Takatori, R. De Dier, J. Vermant, and J. F. Brady, *Nature communications* **7**, 1 (2016).
- [17] P. Dolai, A. Das, A. Kundu, C. Dasgupta, A. Dhar, and K. V. Kumar, *Soft Matter* **16**, 7077 (2020).
- [18] A. B. Slowman, M. R. Evans, and R. A. Blythe, *Phys. Rev. Lett.* **116**, 218101 (2016).
- [19] M. Kourbane-Houssene, C. Erignoux, T. Bodineau, and J. Tailleur, *Phys. Rev. Lett.* **120**, 268003 (2018).
- [20] M. J. Metson, M. R. Evans, and R. A. Blythe, *Journal of Statistical Mechanics: Theory and Experiment* **2020**, 103207 (2020).
- [21] T. Agranov, S. Ro, Y. Kafri, and V. Lecomte, *Journal of Statistical Mechanics: Theory and Experiment* **2021**, 083208 (2021).
- [22] O. Chepizhko and F. Peruani, *Phys. Rev. Lett.* **111**, 160604 (2013).
- [23] D. Levis and L. Berthier, *Phys. Rev. E* **89**, 062301 (2014).
- [24] T. Bertrand, Y. Zhao, O. Bénichou, J. Tailleur, and R. Voituriez, *Phys. Rev. Lett.* **120**, 198103 (2018).
- [25] S. Put, J. Berx, and C. Vanderzande, *Journal of Statistical Mechanics: Theory and Experiment* **2019**, 123205 (2019).
- [26] P. Singh and A. Kundu, *Journal of Physics A: Mathematical and Theoretical* **54**, 305001 (2021).
- [27] P. Rizkallah, A. Sarracino, O. Bénichou, and P. Illien, *Phys. Rev. Lett.* **128**, 038001 (2022).
- [28] O. Granek, Y. Kafri, and J. Tailleur, *Physical Review Letters* **129**, 038001 (2022).
- [29] C. Kurzthaler, C. Devailly, J. Arlt, T. Franosch, W. C. K. Poon, V. A. Martinez, and A. T. Brown, *Phys. Rev. Lett.* **121**, 078001 (2018).
- [30] R. Soto and R. Golestanian, *Phys. Rev. E* **89**, 012706 (2014).
- [31] Y. Fily and M. C. Marchetti, *Phys. Rev. Lett.* **108**, 235702 (2012).
- [32] G. S. Redner, M. F. Hagan, and A. Baskaran, *Phys. Rev. Lett.* **110**, 055701 (2013).
- [33] G. Szamel, *Physical Review E* **90**, 012111 (2014).
- [34] C. Maggi, U. M. B. Marconi, N. Gnan, and R. Di Leonardo, *Scientific reports* **5**, 1 (2015).
- [35] T. GrandPre and D. T. Limmer, *Phys. Rev. E* **98**, 060601 (2018).
- [36] C. Arita, P. L. Krapivsky, and K. Mallick, *Phys. Rev. E* **90**, 052108 (2014).
- [37] In the limit  $\psi \rightarrow 0$  ( $\rho \ll \gamma$ ), the dynamics in fact reduces to the well known simple symmetric exclusion process (SSEP), in which case  $P(g) \sim (1 - \rho)^g$  and the corresponding typical gap size is given by  $g_* = -1/\ln(1 - \rho) \simeq 1/\rho$ , which is the average interparticle spacing.
- [38] S. Chakraborti, T. Chakraborty, A. Das, R. Dandekar, and P. Pradhan, *Phys. Rev. E* **103**, 042133 (2021).
- [39] R. Dandekar, S. Chakraborti, and R. Rajesh, *Phys. Rev. E* **102**, 062111 (2020).
- [40] S. Katz, J. L. Lebowitz, and H. Spohn, *Journal of statistical physics* **34**, 497 (1984).